Fractional Order Generalization of Anomalous Diffusion as a Multidimensional Extension of the Transmission Line Equation

Johnson J. GadElkarim, *Member, IEEE*, Richard L. Magin, *Fellow, IEEE*, Mark M. Meerschaert, Silvia Capuani, Marco Palombo, Anand Kumar, and Alex D. Leow

***Abstract*—In this paper, a new fractional order generalization of the diffusion equation is developed to describe the anisotropy of anomalous diffusion that is often observed in brain tissues using magnetic resonance imaging (MRI). The new model embeds three different fractional order exponents—corresponding to the principal directions of water diffusion—into the governing Bloch–Torrey equation. The model was used to analyze diffusion weighted MRI data acquired from a normal human brain using a 3T clinical MRI scanner. Analysis of the data revealed normal Gaussian diffusion in the cerebral spinal fluid (isotropic fractional order exponent of (0.90 ± 0.1), and anomalous diffusion in both the white (0.67 ± 0.1) and the gray (0.77 ± 0.1) matter. In addition, we observed anisotropy in the fractional exponent values for white mater (0.59 ± 0.1 along the fibers versus 0.68 ± 0.1 across the fibers), but not for gray matter. This model introduces new parameters to describe the complexity of the tissue microenvironment that may be sensitive biomarkers of the structural changes arising in neural tissues with the onset of disease.**

***Index Terms*—Anomalous diffusion, Bloch–Torrey equation, fractional calculus, magnetic resonance imaging.**

I. Introduction

SIGNAL propagation on an *RC* transmission line can be described by a partial differential equation that is equivalent in form to the equations describing classical *Gaussian* diffusion. Fractional order generalizations of this model reflect the onset of anomalous, *non-Gaussian* diffusion. Anomalous diffusion has been characterized in both space and time using a rich variety of fractional order derivatives. The review by Metzler and Klafter [1] provides an excellent historical background for this approach. The mathematical description of the form and properties of fractional order derivatives can be found in the monographs by Podlubny [2], Herrman [3], and Meerschaert and Sikorskii [4]. In addition, an excellent summary of both theoretical models and experimental applications is available in the recent book by Klages *et al.* [5].

Fractional order operators provide a convenient way to generalize the propagation of electrical signals in devices, circuits and networks. Let $P(x,t)$ represent a voltage or current on an electrical transmission line with inductance (L), capacitance (C), and resistance (R)—all expressed per unit length. If we further allow α, β to represent the fractional orders of the Caputo time derivative and the Riesz space derivative, respectively (both derivatives are defined in the Appendix), we can write the classical transmission line equation in the form

$$\frac{\partial^{\alpha} P(x,t)}{\partial t^{\alpha}} = D_{\alpha,\beta} \frac{\partial^{2\beta} P(x,t)}{\partial |x|^{2\beta}} \tag{1}$$

where $D_{\alpha,\beta}$ is a generalized propagation constant with units of $\mathrm{mm}^{2\beta}/\mathrm{s}^{\alpha}$ (e.g., *LC* in the case of a lossless line, and *RC* in the case of a very low inductance telegraph cable). As the overall fractional order of the time and space derivatives span the integer range from 0 to 2, the propagation of both the voltage, $V(x,t)$ and the current $I(x,t)$ along the transmission line smoothly morph from diffusion $(\alpha = 1, \beta = 1)$ to wave propagation $(\alpha = 2, \beta = 1)$.

Diffusion is also characterized through a stochastic model of Brownian motion governed by Fick's second law, which is identical in form to (1). Here, $P(x,t)$ represents the local concentration of diffusing particles, or equivalently, its probability density function—assuming an initial delta distribution of material at $x = 0$ and $t = 0^{+}$, and proper normalization. In this situation, $P(x,t)$, is described as the *diffusion propagator* and the mean squared displacement of the particles grows with time raised to the power, $H = \alpha/2\beta$, here H is the *Hurst index* ($H < 1/2$, subdiffusion; $H = 1/2$, Gaussian diffusion; $H > 1/2$, superdiffusion). Thus, for values other than $H = 1/2$, the diffusion is described as "*anomalous*." By measuring the Hurst index (fractional order) of water diffusion in tissue, we can extract a measure or biomarker for the underlying tissue structure. This structure governs the flow of current (movement of ions) in

Manuscript received February 19, 2013; revised April 11, 2013; accepted April 17, 2013. Date of publication June 19, 2013; date of current version September 09, 2013. The work of R. L. Magin was supported by National Institute of Biomedical Imaging and Bioengineering (NIBIB) R01 Grant EB 007537. The work of M. M. Meerschaert was supported in part by the National Science Foundation (NSF) under Grant DMS-1025486 and in part by the National Institutes of Health (NIH) under Grant R01-EB012079. This paper was recommended by Guest Editor A. Elwakil.

J. J. GadElkarim is with the Electrical and Computer Engineering Department and the Department of Psychiatry, University of Illinois at Chicago, Chicago, IL 60612 USA (e-mail: jgadel2@uic.edu).

R. L. Magin is with the Department of Bioengineering, University of Illinois at Chicago, Chicago, IL 60607 USA (e-mail: rmagin@uic.edu).

M. M. Meerschaert is with the Department of Statistics and Probability, Michigan State University, East Lansing, MI 48824 USA (e-mail: mcubed@stt.msu.edu).

S. Capuani is with the CNR IPCF UOS Roma Sapienza, Physics Department, Sapienza University of Rome, 00185 Rome, Italy (e-mail: silvia.capuani@roma1.infn.it).

M. Palombo is with the Physics Department, Sapienza University of Rome, 00185 Rome, Italy (e-mail: marco.palombo@roma1.infn.it).

A. Kumar is with the Department of Psychiatry, University of Illinois at Chicago, Chicago, IL 60612 USA (e-mail: akumar@psych.uic.edu).

A. D. Leow is with the Department of Psychiatry and the Department of Bioengineering, University of Illinois at Chicago, Chicago, IL 60612 USA (e-mail: alexfeuillet@gmail.com).

Digital Object Identifier 10.1109/JETCAS.2013.2265795

TABLE I
ABBREVIATION AND NOTATION

Abbreviation and Notation

WM	white matter
GM	gray matter
CSF	cerebrospinal fluid
MRI	magnetic resonance imaging
dMRI	diffusion magnetic resonance imaging
DW	diffusion weighted
DT	diffusion tensor
DTI	diffusion tensor imaging
ADC	apparent diffusion coefficient
FA	fractional anisotropy
MD	mean diffusivity
AA^{β}	anomalous anisotropy (for the $\boldsymbol{\beta}$ parameters)
MAE	mean anomalous exponent
LM	Levenberg-Marquardt
PDF	probability density function

$\mathbb{R}^d$	the space of d-tuples of reals $\{x_1 \ldots x_d\}$
$\int \ldots d_d \boldsymbol{x}$	$\int_{\mathbb{R}^d} \ldots dx_1 \ldots dx_2$
$(.)^{\mathrm{T}}$	transpose
x, y, z	coordinate system of the laboratory frame
θ, φ, Ψ	coordinate system described by the principal directions of diffusion
$\boldsymbol{k} = (k_x \ k_y \ k_z)^{\mathrm{T}}$	spatial frequency (wave) vector in Fourier space of the $[x, y, z]$ coordinate system
$\boldsymbol{k'} = (k_\theta \ k_\varphi \ k_\Psi)^{\mathrm{T}}$	spatial frequency (wave) vector in Fourier space of the $[\theta, \varphi, \Psi]$ coordinate system
$F(\boldsymbol{k}) = \Im\{f(\boldsymbol{x})\} = \int f(\boldsymbol{x}) e^{-i\boldsymbol{k}.\boldsymbol{x}} d_d \boldsymbol{k}$	Fourier transform
$f(\boldsymbol{x}) = {}^{1}\!/_{(2\pi)^d} \int F(\boldsymbol{k}) e^{i\boldsymbol{k}.\boldsymbol{x}} d_d \boldsymbol{x}$	inverse Fourier transform

axons and across cell membranes, the distribution of metabolites (sugars, amino acids) in cells and the surrounding extracellular matrix, and the uptake of drugs from capillaries. Fortunately, the magnitude of the electrical signal acquired in MRI is sensitive to the movement of water through local tissue structures as reflected in the detected frequency, relaxation times, and the ADC (note, all abbreviations and definitions are listed in Table I).

The connection between diffusion and magnetic resonance for water protons is described by the Bloch–Torrey equation [6]. Solving the Bloch–Torrey equation for an anisotropic material, such as brain WM, provides the basis for DTI. In DTI, the acquired DW signal, S, is given by the equation

$$S(b, \mathbf{g}) = S_0 \exp(-b\boldsymbol{g}^T \boldsymbol{D} g) \tag{2}$$

where S_0 is the initial signal intensity with very small or no DW, $\boldsymbol{D}$ is a symmetric positive definite 3×3 matrix, called the DT (mm^2/s) with the form

$$\boldsymbol{D} = \begin{bmatrix} D_{xx} & D_{xy} & D_{xz} \\ D_{xy} & D_{yy} & D_{yz} \\ D_{xz} & D_{yz} & D_{zz} \end{bmatrix} \tag{3}$$

$\boldsymbol{g}$ is a unit vector in the direction of the applied magnetic field gradient, and b (s/mm^2) is a user controlled parameter that depends on the timing, duration and strength of the selected gradient pulses [7]. Diagonalization of the DT gives the principal directions of the diffusion process (eigenvectors) and the diffusion coefficient in each direction (eigenvalues: $\lambda_1, \lambda_2, \lambda_3$). Using the extracted eigenvalues, one can compute several metrics that provide valuable information about tissue microstructure [8]. Examples of such metrics are the trace ($\mathrm{TR} = \lambda_1 + \lambda_2 + \lambda_3 = D_{xx} + D_{yy} + D_{zz}$), the MD ($\mathrm{MD} = \mathrm{TR}/3$), and the FA defined as

$$\mathrm{FA} = \sqrt{\frac{(\lambda_1 - \lambda_2)^2 + (\lambda_1 - \lambda_3)^2 + (\lambda_2 - \lambda_3)^2}{2(\lambda_1^2 + \lambda_2^2 + \lambda_3^2)}}. \tag{4}$$

FA varies from zero to one, a value of zero FA indicates isotropic diffusion and an FA of one indicates anisotropic diffusion. In the isotropic case the DT can be written in the form $\boldsymbol{D} = D\boldsymbol{I}$, where $\boldsymbol{I}$ is a 3×3 unit matrix and D is a scalar with the same units as $\boldsymbol{D}$. Hence, (2) becomes

$$S = S_0 \exp(-bD). \tag{5}$$

In brain tissues, D is usually called the ADC and has a value approximately one third that of pure water (2×10^{-3} mm^2/s at room temperature) [9].

In situations where the data deviate from the mono-exponential decay, one can utilize a stretched exponential function of the form

$$S = S_0 \exp(-(b(DDC))^{\alpha}) \tag{6}$$

where *DDC* (mm^2/s) is the *distributed diffusion coefficient*, and α (dimensionless) is the *stretching or anomalous diffusion exponent*, $(0 < \alpha \leq 1)$. This function was introduced by Bennett *et al.* [6] and found to provide an improved fit to the collected data [10]. Hall and Barrick [11] also used a stretched exponential function—derived from a fractal model—to describe diffusion in human brain tissue. In addition, Magin *et al.* [12] generalized the Bloch–Torrey equation by introducing fractional space derivatives of order β and found that the signal decay following a Stejskal–Tanner diffusion pulse sequence could be expressed as a stretched exponential of the form

$$S = S_0 \exp\left(-D\mu^{2(\beta-1)}(\gamma G \delta)^{2\beta}\left(\Delta - \delta\frac{2\beta - 1}{2\beta + 1}\right)\right) \tag{7}$$

where β (dimensionless) is the *stretching exponent* $(0 < \beta \leq 1)$, μ (mm) is a fractional order space constant needed to preserve units, γ (MHz/Tesla) is the gyromagnetic ratio of the proton, G (Tesla/mm) is the magnitude of the applied magnetic field gradient, and Δ(s) and δ(s) are the pulse separation interval and the diffusion gradient duration, respectively [11]. Setting β to unity, one recovers the classical exponential decay model in (5) [9]. By applying this model to trace MRI image data acquired from samples of Sephadex gel with known complexity and tortuosity, the new parameter μ was found to be directly proportional to tortuosity, while β was found to be

inversely proportional to the complexity of the surroundings. In a further study of normal adult brain tissue, Zhou *et al.* [12] found the WM to exhibit lower β values than nearby regions of GM, reflecting the greater complexity and anisotropy of WM compared with GM.

Recently, several studies have examined the directional dependence of the stretched exponential model of anomalous diffusion. Hall and Barrick [13], for example, proposed a two-step anomalous diffusion tensor imaging scheme based on extending the DTI model using a fractional tensor exponent of the form

$$S(b) = S_0 \exp\left(-[b\boldsymbol{g}^T \boldsymbol{A} g]^{(\boldsymbol{g}^T \boldsymbol{\Gamma} \boldsymbol{g})}\right) \tag{8}$$

where $\boldsymbol{A}$ (mm^2/s) and $\boldsymbol{\Gamma}$ (dimensionless) are both rotationally invariant tensors called the *distributed diffusivity tensor* and the *anomalous exponent tensor* respectively. Both tensors are assumed to be symmetric 3×3 matrices and to be described by ellipsoids. Decomposition of both tensors into their corresponding eigenvalues and eigenvectors yields behavior for $\boldsymbol{A}$ that is similar to the classical DT, while the behavior of $\boldsymbol{\Gamma}$ decomposes in a similar manner, but now reflecting the principal directions of tissue complexity. Analysis of human brain data using this model found good correlation between the principal eigenvalue of the diffusion tensor $\boldsymbol{A}$ and highest (closer to one) value of the fractional tensor $\boldsymbol{\Gamma}$, that is, the directions of highest diffusion corresponds to normal Gaussian diffusion [13].

In another study by De Santis *et al.* [14], these workers combined the directional information of DTI with stretched exponential fitting. First, they determined the principal eigenvectors from DTI for each voxel and then they fit the multiple b-value data to three stretched exponentials, each aligned along the principal DTI axes according to the equation

$$S(b) = S_0 \exp\left(-\sum_{i=1}^{3} A_i b^{\gamma_i}\right) \tag{9}$$

where A_i ($\mathrm{mm}^{2\gamma i}/\mathrm{s}^{\gamma i}$) is a generalization of the diffusion constant. In the fitting procedure of (8), De Santis *et al.* assumed a correlation between the principal axis of the DT and the directional dependence of tissue complexity. Using this fitting procedure, De Santis *et al.* reported a strong correlation between anomalous anisotropy (γA) (the mean squared difference between the stretching exponents and their mean values) and DTI FA. Anomalous anisotropy was computed using (5) by replacing λ_i by γ_i. Moreover, a positive correlation was found between MD and the mean value of the stretched exponents ($\mathrm{M}\gamma$).

In summary, the work to date suggests that there is additional information in the directional dependence of the stretched or *anomalous diffusion exponent*. In order to investigate this phenomenon, we solved the fractional order Bloch–Torrey equation in a multidimensional formulation that separates the tissue anisotropy from the directional dependence of the *stretched exponential* parameters.

This paper is organized as follows. First, Section II describes a multidimensional generalization of the fractional Bloch–Torrey equation, and presents a proposed solution. Second, in Section III we describe image acquisition and analysis procedures as well as a new parameter estimation procedure. In Section IV, the new parameters are displayed in the form of brain maps and the supporting statistics are provided. This section is followed by the discussion in Section V. Finally, we have provided a short Appendix with the fundamental definition of both the Caputo and the Riesz fractional derivative. A summary of the tools used for vector fractional calculus and a multidimensional generalization of the fractional diffusion equation are also provided in the Appendix.

II. Theory

A. The Bloch–Torrey Equation

In this paper, we only consider changes in signal intensity due to diffusion. Neglecting Larmor precession and T_1 and T_2 relaxation, the Bloch–Torrey equation describing the magnetization $\boldsymbol{M}(\boldsymbol{r}, t)$ (Amp/mm) of a sample undergoing diffusion in a time varying gradient $\boldsymbol{G}(t)$ can be described by the following equation:

$$\frac{\partial \boldsymbol{M}}{\partial t} = \gamma \boldsymbol{M} \times (\boldsymbol{r} \cdot \boldsymbol{G}(t)) + \nabla^T \boldsymbol{D} \nabla \boldsymbol{M} \tag{10}$$

where γ is the gyromagnetic ratio (42.58 MHz/Tesla for protons), $\boldsymbol{r} = (\,x \quad y \quad z\,)^T$ (mm) is a position vector in the laboratory frame, $\boldsymbol{G}(t) = (\,G_x \quad G_y \quad G_z\,)^T$ (Tesla/mm) is the time-varying applied gradient, $\nabla = (\,\partial/\partial x \quad \partial/\partial y \quad \partial/\partial z\,)^T$ and $\boldsymbol{D}$ is the DT which has the form $D\boldsymbol{I}$ in isotropic diffusion with D being the coefficient of self-diffusion and $\boldsymbol{I}$ a 3×3 unit matrix. In anisotropic diffusion, $\boldsymbol{D}$ is a positive definite symmetric matrix as defined in (3). If we let $M_{xy} = \mathrm{M}_x + i\mathrm{M}_y$, where $i = \sqrt{-1}$, then we can write

$$\frac{\partial M_{xy}}{\partial t} = -i\gamma(\boldsymbol{r} \cdot \boldsymbol{G}) M_{xy} + \nabla^T \boldsymbol{D} \nabla M_{xy}. \tag{11}$$

Following the analysis presented in Abragam [15] and Haacke [16], one assumes a solution to this partial differential equation of the form

$$M_{xy} = M_0 A(t) \exp(-i\boldsymbol{r} \cdot \boldsymbol{L}(t)), \boldsymbol{L}(t) = \gamma \int_0^t \boldsymbol{G}(t'')dt'' \tag{12}$$

where, $M_{xy}(\boldsymbol{r}, 0) = M_0$ and $A(0) = 1$. Substituting (12) into (11), and applying the gradient operator and integrating, we obtain

$$A(t) = \exp\left(-\int_0^t [(\boldsymbol{L}(t''))^T \boldsymbol{D}(\boldsymbol{L}(t''))]dt''\right). \tag{13}$$

In order to remove the explicit time dependence in (13), Stejskal and Tanner proposed a two pulse sequence consisting of a pair rectangular gradient pulses [11]. A Stejskal–Tanner gradient pulse sequence consists of two rectangular gradient pulses (each of duration δ and separated by interval Δ), amplitude $G = ||\boldsymbol{G}||$, and direction $\boldsymbol{g} = \boldsymbol{G}/\|\boldsymbol{G}\|$. For this sequence, (12) and (13) yield

$$M_{xy} = M_0 \exp\left(-(\gamma G \delta)^2 \left(\Delta - \frac{\delta}{3}\right) \boldsymbol{g}^T \boldsymbol{D} g\right). \tag{14}$$

The term $(\gamma G\delta)^2(\Delta - \delta/3)$ is usually referred to as the b value (s/mm^2) [17]. Using (14), we can describe the acquired diffusion signal for a Stejskal–Tanner pulse sequence as

$$S(b, \boldsymbol{g}) = S_0 \exp(-b\boldsymbol{g}^T \boldsymbol{D} g) \tag{15}$$

which for isotropic diffusion reduces to (5).

B. Fractional Order Bloch–Torrey Equation

Assume that the coordinate system described by the principal directions of diffusion $\boldsymbol{r}' = (\theta \quad \phi \quad \psi)^T$ can be related to the laboratory coordinates $\boldsymbol{r} = (x \quad y \quad z)^T$ using a unitary transformation $\boldsymbol{Q}$ (as shown in Table I). Further, let $\boldsymbol{Q}$ be a unitary matrix that diagonalizes the classical DT: $\boldsymbol{D} = \boldsymbol{Q}\Lambda\boldsymbol{Q}^T$, where $\boldsymbol{Q}$ is the matrix whose columns are the eigenvectors of $\boldsymbol{D}$: $\boldsymbol{V}_\theta, \boldsymbol{V}_\phi, \boldsymbol{V}_\psi$, and Λ(mm^2/s) is a diagonal matrix whose entries are the corresponding eigenvalues of $\boldsymbol{D}$: D_θ, D_ϕ, D_ψ.

Hence, as described in Appendix C, the fractional order generalization of (11) can be written in the $\boldsymbol{r}'$ coordinate system in the form

$$\frac{\partial M_{xy}}{\partial t} = -i\gamma(\boldsymbol{r}' \cdot \boldsymbol{G}')M_{xy} + \widetilde{\nabla}^T[\boldsymbol{D_F}]\widetilde{\nabla}M_{xy} \tag{16}$$

where $\boldsymbol{G}' = \boldsymbol{Q}^T\boldsymbol{G}$, and $\widetilde{\nabla}$ is the gradient operator applied in the r' coordinate system, with Fourier symbol $\Im\{\widetilde{\nabla}\} = i\boldsymbol{k}' = i(\,k_\theta \quad k_\phi \quad k_\psi\,)^T$, and $\boldsymbol{D}_F$ is the fractional integral operator as defined in Appendix B acting in the $\boldsymbol{r}'$ coordinate system and having the Fourier symbol as shown in the equation at the bottom of the page. The mu parameters (mm) in the $\boldsymbol{D}_F$ operator are space constants needed to preserve units [18]. We assume a solution to (16) in the form

$$M_{xy} = M_0 A(t)\exp(-i\boldsymbol{r}' \cdot \boldsymbol{L}'(t)), \boldsymbol{L}'(t) = \gamma \int_0^t \boldsymbol{G}'(t'')dt''. \tag{17}$$

Substituting (17) into (16), and applying the above operator, we obtain

$$A(t) = \exp\left(-\int_0^t \sum_h \mu_h^{2\beta_h - 2} D_h |(L'_h(t''))|^{2\beta_h} dt''\right) \tag{18}$$

where $h = \{\theta, \phi, \psi\}, L'_h(t) = \boldsymbol{L}^{\mathrm{T}}(t)\boldsymbol{V}_h$, and $0 < \beta_h \leq 1$ are the stretched exponents. Finally, if we again consider the Stejskal–Tanner gradient pulse pairs, as defined above, we find

$$M_{xy} = M_0 \exp\left(-\sum_h \mu_h^{2\beta_h - 2} D_h |\gamma\delta \boldsymbol{G}^T \boldsymbol{V}_h|^{2\beta_h} \times \left(\Delta - \delta\frac{2\beta_h - 1}{2\beta_h + 1}\right)\right). \tag{19}$$

Using (18), we can describe the acquired signal as follows:

$$S(\boldsymbol{g}, t) = S_0 \exp\left(-\sum_h \mu_h^{2\beta_h - 2} D_h |\gamma\delta \boldsymbol{G^T V}_h|^{2\beta_h} \times \left(\Delta - \delta\frac{2\beta_h - 1}{2\beta_h + 1}\right)\right). \tag{20}$$

Note that when h equals only θ, we recover (7). Moreover, when all of the beta values are set to one, we recover the classical model described in (15) since (20) becomes

$$\begin{aligned} S(b, \boldsymbol{g}) &= S_0 \exp(-b(\boldsymbol{Q}^T\boldsymbol{g})^T \boldsymbol{\Lambda}(\boldsymbol{Q}^T\boldsymbol{g})) \\ &= S_0 \exp(-b\boldsymbol{g}^T\boldsymbol{D}g). \end{aligned} \tag{21}$$

III. Materials and Methods

In order to evaluate the proposed model, multiple b value dMRI scans were acquired from a healthy subject. The subject was scanned on a 3T Siemens "Allegra" scanner equipped with a circularly polarized transmit-receive coil. DW axial images through the optical tracts were acquired using double SE EPI sequences with $\mathrm{TR/TE} = 6400/107$ ms, slice thickness $= 3$ mm, matrix 128×128, $\mathrm{FOV} = 23\times23$ cm^2, bandwidth $= 1860$ Hz/pixel. DW images were acquired at 16 b values, ranging from 0 to 5000 s/mm^2, generated by varying the applied gradient amplitude while fixing the pulse width (δ) and pulse separation (Δ) at 35 and 107 ms, respectively. At each b value, the DW gradient was applied at six noncollinear directions. The whole acquisition took $\sim$20 min.

A. Data Analysis and Model Fitting

All DW images were corrected for eddy current distortions using *FSL* version 4 software (http://www.fmrib.ox.ac.uk/fsl). As a first step, tensor calculations as well as DT diagonalization were performed using the *DTIStudio* program (http://www.mristudio.org) using the $b = 1000$ s/mm^2 subset of the acquired data in order to compute $\boldsymbol{D}$. Afterward, the whole spectrum of b values was used to fit different $\boldsymbol{\mu}$ and $\boldsymbol{\beta}$ values in (20) using the *Levenberg–Marquardt* algorithm implemented in MATLAB R2011a (MathWorks, Natick, MA, USA). The initial $\boldsymbol{\beta}$ values were chosen as 0.75, and the initial $\boldsymbol{\mu}$ values were computed from (20), with $\boldsymbol{\mu}$ being the only variables (the initial values of $\boldsymbol{D}$ and $\boldsymbol{\beta}$ were used in this computation). After determining the initial values, (20) was used to analyze the set of DW images to yield the final values of $\boldsymbol{\beta}$ and $\boldsymbol{\mu}$ on a voxel-by-voxel basis (the fitted results were insensitive to the chosen initial $\boldsymbol{\beta}$ values). In applying the *LM* algorithm, the bounds on all elements of $\boldsymbol{\beta}$ and $\boldsymbol{\mu}$ were taken as $0.5 < \boldsymbol{\beta} \leq 1$ and $0 < \boldsymbol{\mu} < 0.05$ mm. It is assumed that the eigenvalues of the DT are ordered such that: $D_\theta \leq D_\phi \leq D_\psi$. The same order is followed in the

$$\Im\{\boldsymbol{D_F}\} = \begin{pmatrix} \mu_\theta^{2\beta_\theta - 2} D_\theta |k_\theta|^{2\beta_\theta - 2} & 0 & 0 \\ 0 & \mu_\phi^{2\beta_\phi - 2} D_\phi |k_\phi|^{2\beta_\phi - 2} & 0 \\ 0 & 0 & \mu_\psi^{2\beta_\psi - 2} D_\psi |k_\psi|^{2\beta_\psi - 2} \end{pmatrix}.$$

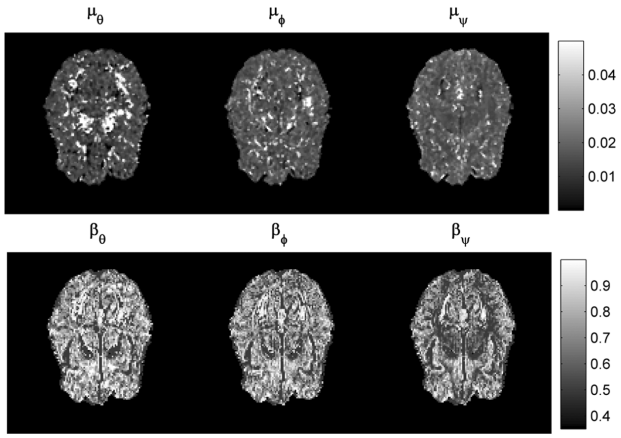

Fig. 1. Spatially resolved maps of the unit preserving space constants (μ_θ, μ_ϕ, and μ_ψ) (top row), and the dimensionless operational order parameters, (β_θ, β_ϕ and β_ψ) (bottom row) in the model described by (20).

TABLE II
MEAN AND STANDARD DEVIATION SUMMARY OF THE FITTED PARAMETERS AND THE COMPUTED METRICS

	GM	WM	CSF
β_θ	0.77 ± 0.1	0.68 ± 0.1	0.87 ± 0.1
β_φ	0.77 ± 0.1	0.68 ± 0.1	0.91 ± 0.02
β_ψ	0.78 ± 0.1	0.59 ± 0.1	0.88 ± 0.1
μ_θ(μm)	16.7 ± 5.5	21.6 ± 5.4	12.7 ± 8.3
μ_φ (μm)	19.8 ± 5.6	23.1 ± 6.3	23.7 ± 12.5
μ_ψ (μm)	24.5 ± 11.3	18.1 ± 6.1	26.6 ± 14.3
MD (μm^2/ms)	0.98 ± 0.18	0.65 ± 0.07	2.66 ± 0.8
FA	0.17 ± 0.08	0.42 ± 0.18	0.13 ± 0.05
MAE	0.77 ± 0.09	0.65 ± 0.07	0.9 ± 0.08
AA$^\beta$	0.07 ± 0.02	0.15 ± 0.05	0.1 ± 0.02
D_θ (μm^2/ms)	0.82 ± 0.18	0.45 ± 0.18	2.33 ± 0.75
D_φ (μm^2/ms)	0.97 ± 0.18	0.7 ± 0.18	2.64 ± 0.83
D_ψ (μm^2/ms)	1.16 ± 0.21	1.11 ± 0.25	3.0 ± 0.96

eigenvector matrix $\boldsymbol{Q}$. To perform the analysis on the resolved parameters of the different types of tissues, WM, GM, and CSF masks were generated using the segmentation tool embedded in the well-known *Statistical Parametric Mapping* (SPM8) software (http://www.fil.ion.ucl.ac.uk/spm/).

IV. RESULTS

Fig. 1 displays maps for the six fitted parameters using the model in (20): the three dimensionless operational order parameters $\boldsymbol{\beta}(\beta_\theta, \beta_\phi, \beta_\psi)$, and the unit-preserving space constants $\boldsymbol{\mu}(\mu_\theta, \mu_\phi, \mu_\psi)$ (with units of mm). A high contrast exists between the GM and WM tissues in the $\boldsymbol{\beta}$ maps. It is qualitatively clear from Fig. 1 that both β_θ and β_ϕ are larger than β_ψ in the WM regions, which is presented in Table II. This result indicates a lower β value in the principal direction of diffusion along the WM fibers.

In order to test the previous result, we have computed AA^β using the same formula used to compute the DTI FA [8]. It is defined as

$$\mathrm{AA}^\beta = \sqrt{\frac{(\beta_\theta - \beta_\phi)^2 + (\beta_\theta - \beta_\psi)^2 + (\beta_\phi - \beta_\psi)^2}{2((\beta_\theta)^2 + (\beta_\phi)^2 + (\beta_\psi)^2)}}. \tag{22}$$

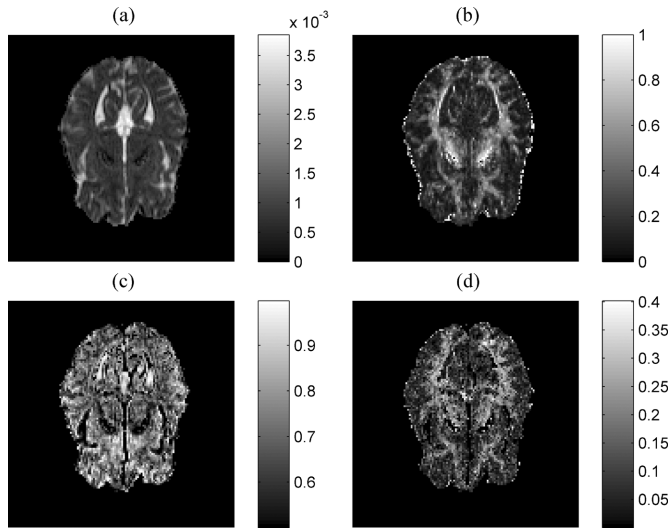

Fig. 2. (a) MD, (b) FA, (c) MAE, and (d) anomalous anisotropy (AA^β) maps.

Fig. 2 shows maps of the conventional FA, MD (computed by averaging the eigenvalues of the DT), MAE (computed by averaging the stretched exponents), as well as AA^β in order to compare our results with De Santis' *et al.* $\mathrm{M}\gamma$ and anomalous anisotropy ($\gamma\mathrm{A}$) presented in the introduction [14]. Indeed, qualitatively, one can see that AA^β has higher values in WM fibers and lower values in GM. These results are similar to those found for γA, which are quantitatively displayed in Table II. Moreover, we report a high correlation between the AA^β and the FA in the WM region with the correlation coefficient being 0.8 and a p-value <0.0001.

V. DISCUSSION

Diffusion MRI is a noninvasive technique that produces images whose contrast is modulated by the random translational motion of water molecules [16]. In biological tissues, where the water can explore the passageways between cells, organelles, membranes and macromolecules, dMRI reflects the heterogeneity of local tissue structure. At every voxel in a DW image, the logarithm of the normalized detected signal (S/S_0) is directly proportional to the ADC at the corresponding location in the brain, as shown in (5). Combining the information from DW images acquired in different gradient directions allows us to infer the principal directions of diffusion as well as the ADC in each of those directions through the diagonalization of the DT. Therefore, dMRI is used clinically to view disruption of the fiber structure of neural tracks in WM disease, and cell death in GM following acute stroke [16], [19].

Fractional order generalization of the multidimensional form of the diffusion equation extends the Bloch–Torrey equation by introducing two new sets of parameters: the fractional order parameters $\boldsymbol{\beta}$ (dimensionless), and the unit preserving space constants $\boldsymbol{\mu}$ (with units of millimeters). Using this approach in human brain, our $\boldsymbol{\beta}$ values (Table II) were found to be lower in WM ($\sim 0.65 \pm 0.1$) than in GM ($\sim 0.77 \pm 0.1$), suggesting a higher complexity in WM. In CSF, the $\boldsymbol{\beta}$ values were found to be close to unity ($\sim 0.9 \pm 0.1$) as expected.

In recent studies [13], [14] that applied the diffusion gradient in different directions researchers found that the value of the stretched exponent was sensitive to gradient direction, particularly in WM. In this paper, we found that the *stretched exponents* were lowest in the direction of the WM fibers, as illustrated in Fig. 1 and 2. In particular, β_Ψ, which represents the stretched exponent in the direction of the principal eigenvector, was found to be lower than β_θ and β_ϕ in WM ($\beta_\Psi \sim 0.59 \pm 0.1$). Moreover, β_θ and β_ϕ were found close in values ($\sim 0.68 \pm 0.1$) in WM regions, which explain the higher anisotropy along WM tracts in the AA^β map (Fig. 2).

The existence of low beta values along the WM fibers may first seem counter intuitive, especially when we try to connect it with the concept of complexity. However, a deeper understanding of the underlying distribution, described in (A10), can explain our result in light of the CTRW model. The stretched exponential model of the anomalous diffusion can be explained by setting α to 1 and solving (1), which will result in an *alpha stable* distribution for the $P(x,t)$. This model is known as the *Lévy flight*, in which particles are allowed to occasionally perform large jumps in their random walks. Alpha stable distributions are heavy tailed functions having power law probability tails $P(|x| > x) \sim x^{-2\beta}$ and their Fourier transform is known to be a stretched exponential [1]. It has been proven that a Fourier relationship exists between the diffusion propagator and the normalized DW signal (S/S_0) under the short pulse assumption (when the pulse separation period $\Delta \gg$ pulse duration δ which holds in the current experiment setup) [20]. Hence, it is expected that a streched exponential relationship in the $\boldsymbol{q}$-space (where $\boldsymbol{q} = \gamma\delta\boldsymbol{G}$ is assumed to be the spatial Fourier frequency of units mm $^{-1}$) described by the acquired DW signal.

According to the CTRW model, the heavy tailed solution for the space fractional diffusion model reflects the probability that distant randomly walking particles could jump to the current position [21]. From Fig. 3, one can deduce that decreasing the *stretched exponents*, $\boldsymbol{\beta}$, will result in stretching the tail of the $P(\boldsymbol{r},t)$ distribution in the corresponding direction [this can be seen when comparing Fig. 3(a) to Fig. 3(c), where a lower β_ϕ has caused a longer tail in the ϕ direction in (c) compared to (a)]. Hence, it is more likely that distant particles along the WM fibers will be able to perform long jumps than particles randomly walking in the transverse directions, which explains the lower beta found in the principal direction of diffusion along the optical fibers in Fig. 1. In order to tie this result to the anatomy of the brain, we postulate the entrapment of water molecules along the WM fibers. When the molecules are freed, they might commit long jumps. Unlike WM, $\boldsymbol{\beta}$ values were isotropic in GM tissues as well as the CSF appearing as low AA^β values in Fig. 2 and similar average values for the stretched exponents in Table II.

The unit preserving constants, $\boldsymbol{\mu}$, were found to follow the same trend previously reported when the Magin *et al.* isotropic model [18] was used to study brain tissues [12], [22], although they did not show a good tissue contrast (Fig. 1) unlike what have been reported for the μ map in [12]. The $\boldsymbol{\mu}$ parameters exhibit higher values in WM compared to GM tissues in all directions. Instability was seen in the fitting for CSF voxels where the diffusion process approaches the normal case with $\boldsymbol{\beta}$ values

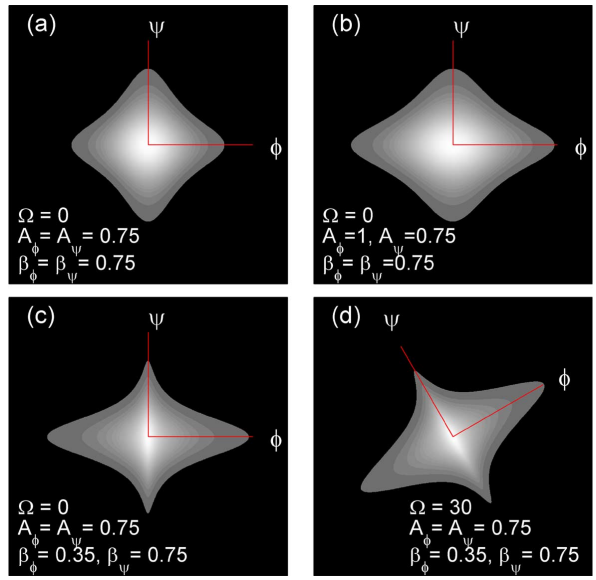

Fig. 3. Contour plot (isomap) of different versions of a 2-D version of $C(\boldsymbol{r},t)$ by varying five parameters (two scale parameters: A_ϕ and A_ψ, rotation angle: Ω, and two stretched exponents: β_ϕ and β_ψ). Coordinate system is shown in red.

closer to unity, as evidenced by the large standard deviations in Table II. The blurriness in the $\boldsymbol{\mu}$ maps may be due to the low SNR (around 1.25 in GM and around 1.4 for WM at a b value of 5000 s/mm^2) of the acquired data compared to that used in [12] (reported to be around 3.5 in GM and around 6 for WM at a b value of 4700 s/mm^2). Indeed, fitting our data to the Magin *et al.* model resulted in a blurred μ map. In general, we posit that both fitting the μ parameter in the isotropic model or the $\boldsymbol{\mu}$ parameters in our anisotropic model are sensitive to the SNR of the data. Moreover, increasing SNR without sacrificing resolution requires averaging multiple acquisitions, which increases the acquisition time.

Overall, our results reflect the existence of three different diffusion phenomena occurring in brain tissue. The first—diffusion in anisotropic media—depends on the structure and composition of the environment in which the water molecules move. Barriers such as macromolecules, membranes, and bundles of axons will create a restricted diffusive medium in which the directions of allowed motion are constrained causing a reduction in the measured ADC, when compared with a barrier-free environment. The second—diffusion in multi-scale or fractal structures—has been demonstrated to occur in brain tissue that exhibits fractal-like appearance [23]–[26], and thus it has been linked to the use of fractional order *stretched exponents* (which quantify sub-diffusion processes in terms of random walk particle trajectories). Such a process could shed light on the relationship between subdiffusion and the anisotropy found in the fractional order parameters [18], [25], [27], [28]. The third—diffusion in porous heterogeneous media—is related to the anomalous diffusion description for which $H > 1/2$ or $<1/2$ [1]. This could be due to the complexity of the random walk executed by the spins (water protons) caused by magnetic susceptibility differences between different tissues, water compartments and chaotic travel paths [29]–[31].

Finally, it is important to note that our model has two main limitations. First, similar to DTI, the model does not take into consideration partial volume contamination inside a voxel where multi-fiber crossings are known to influence the principal direction of diffusion, which then skews the fitted FA values. A suggested solution is the utilization of spherical harmonics in order to solve for fiber crossing. However, this would complicate the formulation of the problem. Second, a long processing time is required in order to fit the six fractional order parameters. On a 3 GHz Intel core 2 Duo machine equipped with 8 GB RAM, Matlab based built-in LM implementation takes about 3 min per slice to fit for all parameters. This time could be significantly reduced by using a more efficient C++ based *LM* fitting method, such as the NAG library (http://www.nag.co.uk), which can render the model suitable for group studies.

In conclusion, we have developed a new model based on the fractional order generalization of the Bloch–Torrey equation that is capable of measuring anisotropy due to anomalous diffusion. In future studies, we plan to test the model using phantoms with known structural complexity and anisotropy, and to investigate the utility of using these parameters as a new imaging biomarker in animal and clinical studies.

APPENDIX

A. Fractional Derivatives

For real values of α in the range $0 < \alpha < 1$, the Caputo fractional derivative is defined as [3]

$$ {}_C D^{\alpha} f(t) = \frac{1}{\Gamma(1-\alpha)} \int_0^t \frac{f^{(1)}(t')}{(t-t')^{\alpha}} dt' \tag{A1} $$

where $f^{(1)}(t)$ is the first derivative of $f(t)$. For real values of β in the range $0 < \beta < 2$, the Riesz fractional derivative is defined as [3]

$$ {}_{RZ} D^{\beta} f(x) = \Gamma(1+\beta) \frac{\sin(\pi\beta/2)}{\pi} \times \int_0^{\infty} \frac{f(x+t) - 2f(x) + f(x-t)}{t^{(\beta+1)}} dt. \tag{A2} $$

Using the Fourier transform, a simpler definition of the Riesz derivative can be stated in the form [5]

$$ {}_{RZ} D^{\beta} \{f(x)\} = \Im^{-1} \{-|k|^{\beta} F(k)\}. \tag{A3} $$

For example, when $f(x) = \exp(iax)$, its Fourier transform is $F(k) = 2\pi\delta(k-a)$, and then using (A3), it is easy to compute

$$ {}_{RZ} D^{\beta} \{e^{iax}\} = -|a|^{\beta} e^{iax}. \tag{A4} $$

B. Fractional Vector Calculus

In this section, we extend the theory of fractional vector calculus, presented in [32], to allow the order of the fractional derivative to change with the coordinate direction in an arbitrary orthogonal coordinate system. The usual model for anisotropic diffusion is

$$ \frac{\partial P(\boldsymbol{r}, t)}{\partial t} = \nabla^T \boldsymbol{D} \nabla P(\boldsymbol{r}, t) \tag{A5} $$

where $\boldsymbol{D}$ is a symmetric positive definite matrix (an order 2 tensor). The simplest case is when $\boldsymbol{D}$ is $D\boldsymbol{I}$, where $\boldsymbol{I}$ is a 3×3 identity matrix, and D is a scalar, then we can write

$$ \frac{\partial C(\boldsymbol{r}, t)}{\partial t} = D \nabla^T \nabla P(\boldsymbol{r}, t) = D \Delta P(\boldsymbol{r}, t) \tag{A6} $$

where $\nabla^T \nabla = \Delta$ is the Laplacian operator.

Since the gradient has Fourier symbol $(i\boldsymbol{k})$, we can write $(i\boldsymbol{k}) \cdot F(\boldsymbol{k})$ as the Fourier transform of $\nabla f(\boldsymbol{r})$ where $F(\boldsymbol{k})$ is the vector Fourier transform of the function $f(\boldsymbol{r})$ in terms of the wave vector $\boldsymbol{k} = [\, k_x \quad k_y \quad k_z \,]^T$. Then, the Laplacian has the Fourier symbol $(i\boldsymbol{k})^T (i\boldsymbol{k}) = -(k_x^2 + k_y^2 + k_z^2)$. If $\boldsymbol{D}$ is a diagonal tensor

$$ \boldsymbol{D} = \begin{bmatrix} D_x & 0 & 0 \\ 0 & D_y & 0 \\ 0 & 0 & D_z \end{bmatrix} $$

then $\nabla^T \boldsymbol{D} \nabla$ has the Fourier symbol

$$ (i\boldsymbol{k})^T \boldsymbol{D} (i\boldsymbol{k}) = -\left(D_x k_x^2 + D_y k_y^2 + D_x k_z^2 \right). $$

Let the fractional dispersion tensor $\boldsymbol{D}_F$ be a fractional integration tensor of order $2\beta - 2$. More generally, to allow the order of the fractional derivative to vary with the coordinate, we can take $\boldsymbol{D}_F$ to be the operator with Fourier symbol, as shown in the equation at the bottom of the page. Then, it follows that the dispersion operator $\nabla^T \boldsymbol{D_F} \nabla$ has Fourier symbol

$$ (i\boldsymbol{k})^T \Im\{\boldsymbol{D_F}\}(i\boldsymbol{k}) = -(\mu_x^{2\beta_x - 2} D_x |k_x|^{2\beta_x} + \mu_y^{2\beta_y - 2} D_y |k_y|^{2\beta_y} + \mu_z^{2\beta_z - 2} D_z |k_z|^{2\beta_z}). $$

This operator applies a one dimensional fractional Riesz derivative of a different order in each coordinate. Applying formula (A4) in each coordinate direction we obtain

$$ \nabla^T [\boldsymbol{D_F}] \nabla e^{-i\boldsymbol{r}\cdot\boldsymbol{a}} = \left(- \sum_{j=\{x,y,z\}} \mu_j^{2\beta_j - 2} D_j |a_j|^{2\beta_j} \right) e^{-i\boldsymbol{r}\cdot\boldsymbol{a}}. \tag{A7} $$

$$ \Im\{\boldsymbol{D_F}\} = \begin{pmatrix} \mu_x^{2\beta_x - 2} D_x |k_x|^{2\beta_x - 2} & 0 & 0 \\ 0 & \mu_y^{2\beta_y - 2} D_y |k_y|^{2\beta_y - 2} & 0 \\ 0 & 0 & \mu_z^{2\beta_z - 2} D_z |k_z|^{2\beta_z - 2} \end{pmatrix}. $$

C. Multidimensional Fractional Diffusion Equation

In this section, we will define a multidimensional fractional diffusion equation based on the mathematical notations introduced in Appendixes A and B. Let $P(\boldsymbol{r},t)$ be the *diffusion propagator* of the diffusing particles, which represents the probability of finding a particle at location $\boldsymbol{r}$ and time t such that $P(\boldsymbol{r},t=0)=\delta(\boldsymbol{r})$. Assuming that the principal directions of diffusion coincide with the laboratory coordinates, the new fractional diffusion equation can be written in the form

$$\frac{\partial P(\boldsymbol{r},t)}{\partial t}=\nabla^T \boldsymbol{D_F}\nabla P(\boldsymbol{r},t) \tag{A8}$$

where $\boldsymbol{D}_F$ is a fractional dispersion tensor as defined in Appendix B, and ∇ is the usual gradient operator. Taking the Fourier transform of (A8), we obtain

$$\frac{\partial P(\boldsymbol{k},t)}{\partial t}=\left(-\sum_{j=\{x,y,z\}}\mu_j^{2\beta_j-2}D_j|k_j|^{2\beta_j}\right)P(\boldsymbol{k},t) \tag{A9}$$

where the β_j are dimensionless operational order parameters, and the μ_j are unit preserving space constants. Assuming $P(\boldsymbol{k},0)=1$, the solution to (A9) is

$$P(\boldsymbol{k},t)=\exp\left(-t\sum_{j=\{x,y,z\}}\mu_j^{2\beta_j-2}D_j|k_j|^{2\beta_j}\right). \tag{A10}$$

Equation (A10) describes the characteristic function of a multidimensional operator stable Lévy distribution with independent alpha stable distributions in each coordinate, each with a different stretched exponent. This is more general than the conventional multivariate alpha stable PDF, which applies the same stretched exponent in all directions. For more details, see [4, Ch. 6].

In order to gain a better understanding of the solution in (A10), which represents the Fourier transform of the solution of (A8), we need to take a closer look at the PDF $P(\boldsymbol{r},t)$ that underlies the model. For simplicity, we write the characteristic function in a 2-D form of $P(\boldsymbol{r},t)$ with $t=1$ oriented in a rotated coordinate system $\{\phi,\psi\}$ by an angle Ω in the form

$$P(\boldsymbol{k},t=1)=\exp\left(-\left[A_\phi|k_\phi|^{2\beta_\phi}+A_\psi|k_\psi|^{2\beta_\psi}\right]\right) \tag{A11}$$

where A_ϕ and A_ψ are scale constants ≥ 0, β_ϕ and β_ψ are the stretched exponents, and

$$\begin{bmatrix}k_\phi\\k_\psi\end{bmatrix}=\begin{bmatrix}\cos(\Omega)&\sin(\Omega)\\-\sin(\Omega)&\cos(\Omega)\end{bmatrix}\begin{bmatrix}k_x\\k_y\end{bmatrix}. \tag{A12}$$

The PDF was numerically evaluated in MATLAB by varying the five parameters: $A_\phi, A_\psi, \Omega, \beta_\phi$, and β_ψ in (A11) and then the inverse Fourier transform was computed in order to display its value in the space domain. Note that the rotation matrix used as the relationship between the $\{k_x,k_y\}$ and $\{k_\phi,k_\psi\}$ coordinate systems in the Fourier domain can be used to relate the $\{x,y\}$ and $\{\phi,\psi\}$ coordinate systems in the space domain.

It is clear from Fig. 3 that increasing the scale parameters will increase the spread in the corresponding direction [(b) compared to (a)], while lowering one of the stretched exponents will elongate the tail in the corresponding direction [(c) compared to (a)]. Finally the change of the rotation angle will change the principal axes of the function [(d) compared to (a), (b), and (c)].

ACKNOWLEDGMENT

The authors would like to acknowledge the useful discussions with Y. Sui and C. Ingo regarding the fitting procedure.

REFERENCES

[1] R. Metzler and J. Klafter, "The random walk's guide to anomalous diffusion: A fractional dynamics approach," *Phys. Rep.*, vol. 339, pp. 1–77, 2000.

[2] I. Podlubny, *Fractional Differential Equations: An Introduction to Fractional Derivatives, Fractional Differential Equations, Some Methods of Their Solution and Some of Their Applications*. New York: Academic, 1999.

[3] R. Herrmann, *Fractional Calculus an Introduction for Physicists*. Singapore: World Scientific, 2011.

[4] M. Meerschaert and A. Sikorskii, *Stochastic Models for Fractional Calculus*. Berlin, Germany: De Gruyter, 2011.

[5] R. Klages, G. Radons, and I. M. Sokolov, *Anomalous Transport: Foundations and Applications*. Weinheim, Germany: Wiley-VCH, 2008.

[6] H. C. Torrey, "Bloch equations with diffusion terms," *Phys. Rev.*, vol. 104, pp. 563–565, 1956.

[7] P. J. Basser, J. Mattiello, and D. LeBihan, "Estimation of the effective self-diffusion tensor from the NMR spin echo," *J. Magn. Reson. B*, vol. 103, pp. 247–254, Mar. 1994.

[8] P. J. Basser and C. Pierpaoli, "Microstructural and physiological features of tissues elucidated by quantitative-diffusion-tensor MRI," *J. Magn. Reson. B.*, vol. 111, pp. 209–219, June 1996.

[9] D. Le Bihan, E. Breton, D. Lallemand, P. Grenier, E. Cabanis, and M. Laval-Jeantet, "MR imaging of intravoxel incoherent motions: Application to diffusion and perfusion in neurologic disorders," *Radiology*, vol. 161, pp. 401–407, Nov. 1986.

[10] K. M. Bennett, K. M. Schmainda, R. T. Bennett, D. B. Rowe, H. Lu, and J. S. Hyde, "Characterization of continuously distributed cortical water diffusion rates with a stretched-exponential model," *Magn. Reson. Med.*, vol. 50, pp. 727–734, Oct. 2003.

[11] E. O. Stejskal and J. E. Tanner, "Spin diffusion measurements: Spin echoes in the presence of a time-dependent field gradient," *J. Chem. Phys.*, vol. 42, pp. 288–292, 1965.

[12] X. J. Zhou, Q. Gao, O. Abdullah, and R. L. Magin, "Studies of anomalous diffusion in the human brain using fractional order calculus," *Magn. Reson. Med.*, vol. 63, pp. 562–569, Mar. 2010.

[13] M. G. Hall and T. R. Barrick, "Two-step anomalous diffusion tensor imaging," *NMR Biomed.*, vol. 25, pp. 286–294, Feb. 2012.

[14] S. De Santis, A. Gabrielli, M. Bozzali, B. Maraviglia, E. Macaluso, and S. Capuani, "Anisotropic anomalous diffusion assessed in the human brain by scalar invariant indices," *Magn. Reson. Med.*, vol. 65, pp. 1043–1052, Apr. 2011.

[15] A. Abragam, *The Principles of Nuclear Magnetism*. Oxford, U.K.: Clarendon, 1961.

[16] E. M. Haacke, *Magnetic Resonance Imaging: Physical Principles and Sequence Design*. New York: Wiley, 1999.

[17] D. LeBihan and E. Breton, "Imagerie de diffusion In vivo par Résonance magnétique nucléaire," *CR Académie des Sciences de Paris*, vol. 301, pp. 1109–1112, 1985.

[18] R. L. Magin, O. Abdullah, D. Baleanu, and X. J. Zhou, "Anomalous diffusion expressed through fractional order differential operators in the Bloch-Torrey equation," *J. Magn. Reson.*, vol. 190, pp. 255–270, 2008.

[19] D. Le Bihan, J. F. Mangin, C. Poupon, C. A. Clark, S. Pappata, N. Molko, and H. Chabriat, "Diffusion tensor imaging: Concepts and applications," *J. Magn. Reson. Imag.*, vol. 13, pp. 534–546, Apr. 2001.

[20] E. O. Stejskal, "Use of spin echoes in a pulsed magnetic-field gradient to study anisotropic, restricted diffusion and flow," *J. Chem. Phys.*, vol. 43, pp. 3597–3603, 1965.

[21] R. Schumer, M. M. Meerschaert, and B. Baeumer, "Fractional advection-dispersion equations for modeling transport at the Earth surface," *J. Geophys. Res.-Earth Surface*, vol. 114, Dec. 18, 2009.

[22] Q. Gao, G. Srinivasan, R. L. Magin, and X. J. Zhou, "Anomalous diffusion measured by a twice-refocused spin echo pulse sequence: Analysis using fractional order calculus," *J. Magn. Reson. Imag.*, vol. 33, pp. 1177–1183, May 2011.
[23] F. Caserta, W. D. Eldred, E. Fernandez, R. E. Hausman, L. R. Stanford, S. V. Bulderev, S. Schwarzer, and H. E. Stanley, "Determination of fractal dimension of physiologically characterized neurons in two and three dimensions," *J. Neurosci. Methods*, vol. 56, pp. 133–144, Feb. 1995.
[24] S. Havlin, S. V. Buldyrev, A. L. Goldberger, R. N. Mantegna, S. M. Ossadnik, C. K. Peng, M. Simons, and H. E. Stanley, "Fractals in biology and medicine," *Chaos Solitons Fractals*, vol. 6, pp. 171–201, 1995.
[25] E. Ozarslan, P. J. Basser, T. M. Shepherd, P. E. Thelwall, B. C. Vemuri, and S. J. Blackband, "Observation of anomalous diffusion in excised tissue by characterizing the diffusion-time dependence of the MR signal," *J. Magn. Reson.*, vol. 183, pp. 315–323, Dec. 2006.
[26] T. G. Smith Jr., T. N. Behar, G. D. Lange, W. B. Marks, and W. H. Sheriff Jr., "A fractal analysis of cultured rat optic nerve glial growth and differentiation," *Neuroscience*, vol. 41, pp. 159–166, 1991.
[27] M. G. Hall and T. R. Barrick, "From diffusion-weighted MRI to anomalous diffusion imaging," *Magn. Reson. Med.*, vol. 59, pp. 447–455, Mar. 2008.
[28] E. Ozarslan, T. M. Shepherd, C. G. Koay, S. J. Blackband, and P. J. Basser, "Temporal scaling characteristics of diffusion as a new MRI contrast: Findings in rat hippocampus," *Neuroimage*, vol. 60, pp. 1380–1393, Apr. 2, 2012.
[29] S. Capuani, M. Palombo, A. Gabrielli, A. Orlandi, B. Maraviglia, and F. S. Pastore, "Spatio-temporal anomalous diffusion imaging: Results in controlled phantoms and in excised human meningiomas," *Magn. Reson. Imag.*, vol. 31, pp. 359–365, Apr. 2012.
[30] M. Palombo, A. Gabrielli, S. De Santis, C. Cametti, G. Ruocco, and S. Capuani, "Spatio-temporal anomalous diffusion in heterogeneous media by nuclear magnetic resonance," *J. Chem. Phys.*, vol. 135, pp. 034504–, July 21, 2011.
[31] M. Palombo, A. Gabrielli, S. De Santis, and S. Capuani, "The gamma parameter of the stretched-exponential model is influenced by internal gradients: Validation in phantoms," *J. Magn. Reson.*, vol. 216, pp. 28–36, Mar. 2012.
[32] M. M. Meerschaert, J. Mortensen, and S. W. Wheatcraft, "Fractional vector calculus for fractional advection—Dispersion," *Physica A: Stat. Mechan. Appl.*, vol. 367, pp. 181–190, 2006.

Johnson J. GadElkarim (M'04) received the B.S.E.E. degree from Cairo University, Cairo, Egypt, in 2004, and the M.S.E.E. degree, in 2013, from University of Illinois at Chicago, Chicago, IL, USA, where he is currently working toward the Ph.D. degree in electrical and computer engineering.

Previously, he worked as a Senior Training Engineer in Alcatel-Lucent (2006–2009). Currently, he is pursuing research with the Department of Psychiatry, at University of Illinois at Chicago, Chicago, IL, USA. His research interests include magnetic resonance imaging, diffusion imaging, anomalous diffusion, and brain network analysis.

Richard Magin (M'69–SM'81–F'96) received the B.S. and M.S. degrees in physics from the Georgia Institute of Technology, Atlanta, GA, USA, in 1969 and 1972, respectively. He received the Ph.D. degree in biophysics from the University of Rochester, Rochester, NY, USA, in 1976.

Currently, he is Distinguished Professor of Bioengineering at the University of Illinois at Chicago, Chicago, IL, USA. His research interests focus on the application of magnetic resonance imaging in science and engineering. He served as Editor for the Critical Reviews in Biomedical Engineering (2005–2010).

Prof. Magin is a member of the Biomedical Engineering Society and of the International Society of Magnetic Resonance in Medicine. He is a Fellow of the American Institute for Medical and Biological Engineering. In 2005 he received a Fulbright award for research and teaching in Kosice, Slovakia.

Mark M. Meerschaert received the B.S., M.S., and Ph.D. degrees in mathematics from the University of Michigan, Ann Arbor, MI, USA, in 1977, 1979, and 1984, respectively.

He is currently Probability Editor for the Proceedings of the American Mathematical Society, and a Professor in the Department of Statistics and Probability at Michigan State University. He has served as Chair of this department, Chair of Applied Mathematics at the University of Otago, Dunedin, New Zealand, Professor of Physics and Professor of Mathematics at the University of Nevada, Reno, NV, USA, and Assistant Professor of Mathematics at Albion College. He has authored: Stochastic Models for Fractional Calculus (Berlin: De Gruyter, 2011) with A. Sikorskii; Limit Distributions for Sums of Independent Random Vectors: Heavy Tails in Theory and Practice (New York, NY: Wiley, 2001) with H-.P. Scheffler; and Mathematical Modeling, (Boston, MA: Academic Press, 2013).

Silvia Capuani received the Ph.D. degree in physics from Sapienza University of Rome, Rome, Italy, in 2000.

She is a physicist who has been working in the magnetic resonance field for more than 20 years at the physics department of Sapienza University of Rome, Italy. Her research interests include theoretical speculation and experimental investigation in the field of magnetic resonance diffusion, magnetic resonance imaging applied to investigate porous systems, bone, living tissues, brain and to develop new diagnostic protocols.

Marco Palombo received the B.S. and M.S. degrees in physics, in 2007 and 2010, respectively, from Sapienza University of Rome, Rome, Italy, where he is currently working toward the Ph.D. degree in biophysics.

He is currently pursuing research with the Department of Physics and the Department of Chemistry, at the Sapienza University of Rome, Rome, Italy. His research interests include magnetic resonance imaging, conventional and advanced diffusion imaging, study of anomalous diffusion in complex media, medical imaging, and brain connectivity analysis.

Anand Kumar received the M.B.B.S. degree from Madras Medical College, Madras, India, in 1980. In 1986, he finished his residency from the University of Michigan, Michigan, USA. In 1989, he received the fellowship in clinical neurosciences from the National Institute on Aging.

Currently, he is Lizzie Gilman Professor and Head of the Department of Psychiatry, University of Illinois at Chicago College of Medicine. Previously, he worked as an Assistant Professor of Psychiatry in University of Pennsylvania School of Medicine (1989–1995), Associate Professor of Psychiatry and Associate Director at the Section of Geriatric Psychiatry (1995–1998), and as an Associate Professor in Residence at the University of California at Los Angeles (UCLA) School of Medicine (1998–2001). From 2000 to 2004, he held the position of the Director of the Geriatric Ambulatory Care Program at Neuropsychiatric Hospital. He also was the Director for the division of Geriatric Psychiatry at the UCLA Neuropsychiatric Institute (2004–2008). He has also extensively published in the field of neuropsychiatry. He is an Associate Editor of the *American Journal of Geriatric Psychiatry*.

Dr. Kumar is a reviewer for the Alzheimer's Association Scientific Review Committee, the Chairman of the Scientific Program Committee at the American Association for Geriatric Psychiatry's Annual Conference, and the Site Director and a member of the Board of Directors for the National Network of Depression Centers.

Alex Leow received the Ph.D. degree in biomathematics from the University of California at Los Angeles (UCLA), Los Angeles, CA, USA, in 2003. She received residency training in psychiatry at the Neuropsychiatric Institute and post-graduate research fellowship training at the Laboratory of Neuro Imaging (LONI), both at UCLA.

In addition, she is also a medical doctor and is board-certified in adult psychiatry (the American Board of Psychiatry and Neurology) since 2012. In addition to managing a successful practice in neuropsychopharmacology, she has extensively published in the field of computational neuroimaging and its application in neuropsychiatry, and is currently on the faculty of the Departments of Psychiatry and Bioengineering at the University of Illinois at Chicago, Chicago, IL, USA.

Dr. Leow was a recipient of 2009 NARSAD young investigator award.